Chemical Science

ROYAL SOCIETY OF CHEMISTRY

EDGE ARTICLE

View Article Online
View Journal | View Issue

Cite this: *Chem. Sci.*, 2022, **13**, 1725

All publication charges for this article have been paid for by the Royal Society of Chemistry

Received 20th October 2021
Accepted 14th January 2022

DOI: 10.1039/d1sc05784g

rsc.li/chemical-science

EDOT-based conjugated polymers accessed *via* C–H direct arylation for efficient photocatalytic hydrogen production†

Zhi-Rong Tan,[a] Yu-Qin Xing,[a] Jing-Zhao Cheng,[a] Guang Zhang,[b] Zhao-Qi Shen,[a] Yu-Jie Zhang,[a] Guangfu Liao,[c] Long Chen[b] and Shi-Yong Liu*[a]

3,4-Ethylene dioxythiophene (EDOT), as a monomer of commercial conductive poly(3,4-ethylene dioxythiophene) (PEDOT), has been facilely incorporated into a series of new π-conjugated polymer-based photocatalysts, *i.e.*, BSO_2–EDOT, DBT–EDOT, Py–EDOT and DFB–EDOT, through atom-economic C–H direct arylation polymerization (DArP). The photocatalytic hydrogen production (PHP) test shows that donor–acceptor (D–A)-type BSO_2–EDOT renders the highest hydrogen evolution rate (HER) among the linear conjugated polymers (CPs) ever reported. A HER up to 0.95 mmol h^{-1}/6 mg under visible light irradiation and an unprecedented apparent quantum yield of 13.6% at 550 nm are successfully achieved. Note that the photocatalytic activities of the C–H/C–Br coupling-derived EDOT-based CPs are superior to those of their counterparts derived from the classical C–Sn/C–Br Stille coupling, demonstrating that EDOT is a promising electron-rich building block which can be facilely integrated into CP-based photocatalysts. Systematic studies reveal that the enhanced water wettability by the integration of polar BSO_2 with hydrophilic EDOT, the increased electron-donating ability by O–C p–π conjugation, the improved electron transfer by D–A architecture, broad light harvesting, and the nano-sized colloidal character in a H_2O/NMP mixed solvent rendered BSO_2–EDOT as one of the best CP photocatalysts toward PHP.

Introduction

Photocatalytic water splitting is considered as one of the most promising technologies for converting solar energy into clean hydrogen fuels.[1] Since Fujishima and Honda reported the photocatalytic hydrogen production (PHP) from TiO_2-based photoelectrodes,[2] many inorganic semiconducting materials have been explored for photocatalysis.[3] However, some inherent drawbacks of inorganic photocatalysts still remain, which mainly involve poor response toward visible light and limited tuneability of energy gaps owing to the rigid structures. In recent years, π-conjugated polymers (CPs), as a kind of "soft" photocatalyst that contains only lightweight elements,[4] have attracted extensive attention for photocatalysis due to their broad flexibility in molecular structures, synthetic methods, light absorption, and energy levels.[5–13] Exploiting high-performance CP-based photocatalysts which can be facilely constructed from commonly used building blocks is still a key task waiting to be tackled.

Thiophene and its derivatives are among the most important building blocks in organic electronics, *e.g.*, organic photovoltaics (OPVs) and organic field effect transistors (OFETs),[14,15] owing to their appropriate aromatic stabilization energy (ASE) and electron-donating ability. Among them, 3,4-ethylene dioxythiophene (EDOT) is the monomer of poly(3,4-ethylenedioxythiophene):poly(styrene sulfonate) (PEDOT:PSS), one of the most widely utilized conductive polymers[16,17] in organic electronics.[18–22] As a typical electron-donating unit, EDOT has not yet been used in CP-based photocatalysts. On the other hand, CPs are usually constructed *via* classical Suzuki or Stille C–M/C–Br couplings (M = B or Sn) which require additional preparation of C–M precursors. In recent years, tin- & boron-free C–H direct arylation (*i.e.*, C–H/C–Br coupling) has emerged as an atom-economic protocol for synthesizing π-conjugated materials.[23–27] Our group has synthesized new CPs by C–H direct arylation polymerization (DArP) for PHP applications,[28] which, however, still suffer from lower photocatalytic activities than their counterparts derived from the classical Stille coupling owing to the relatively lower polymerization efficiency of DArP.[29]

[a]*Jiangxi Provincial Key Laboratory of Functional Molecular Materials Chemistry, Department of Chemistry, Jiangxi University of Science and Technology, Ganzhou 341000, China. E-mail: chelsy@zju.edu.cn; chelsy@jxust.edu.cn*

[b]*Department of Chemistry, Tianjin Key Laboratory of Molecular Optoelectronic Sciences, Tianjin University, Tianjin 300072, China*

[c]*Engineering Research Center of Nano-Geomaterials of Ministry of Education, China University of Geosciences, Wuhan 430074, China*

† Electronic supplementary information (ESI) available. See DOI: 10.1039/d1sc05784g

In this work, a facile DArP synthetic strategy was employed to synthesize a series of EDOT-based CPs, *i.e.*, BSO_2–EDOT, DBT–EDOT, Py–EDOT and DFB–EDOT. PHP performances of these CPs were systematically investigated. Among them, donor–acceptor (D–A)-type BSO_2–EDOT achieved a remarkable hydrogen evolution rate (HER) up to 0.95 mmol h^{-1}/6 mg under visible light irradiation. Both the balloon-inflating and water-displacing experiments visually demonstrated that 3 mg of $ETSO_2$–EDOT can produce 100 ml of H_2 gas in 3 h. Encouragingly, the PHP activities of CPs from DArP were superior to the analogues synthesized *via* Stille coupling, demonstrating that DArP is more advantageous to prepare EDOT-based CPs than the classical C–M/C–Br couping. Detailed analysis of the chemical and electronic properties reveals that EDOT has several beneficial effects on CPs: the regioselective α-C–H arylation, enhanced hydrophilicity of the CPs and increased electron-donating ability by C–O polar bonds and p–π conjugation. In contrast to previously exploited polycyclic pyrene[7,29] and electron-accepting sulfones,[30–34] the electron-donating moieties, *e.g.*, thiophene derivatives, have often been overlooked. In this context, we believe that EDOT here reported will become an attractive and universal electron-donating π unit which can be facilely integrated into CPs *via* the atom-economic C–H/C–Br coupling, and paves the way for the green synthesis of high-performance polymeric photocatalysts.

Results and discussion

Synthesis, structural characterization, and morphologies

Four new CPs (Scheme 1), *i.e.* BSO_2–EDOT, DBT–EDOT, Py–EDOT and DFB–EDOT, were smoothly synthesized *via* Pd-catalyzed DArP[28,35] from EDOT and different aryl bromides, including 3,7-dibromodibenzothiophene-5,5-dioxide ($BTSO_2$), 3,7-dibromodibenzo[*b*,*d*]thiophene (BTS), 1,3,6,8-tetrabromopyrene (TBPy) and 1,4-dibromo-2,5-difluorobenzene (DBFB). Note that both the C–H bonds on EDOT can be effectively arylated with various aryl bromides. The ethylene dioxy group at the 3,4-positions of EDOT allows α-C–H bonds to be the exclusive sites toward arylation, which affords regioregular CPs in excellent yields (see the Experimental section). The as-prepared CPs are insoluble in common organic solvents such as MeOH, toluene, dichloromethane and chloroform (Fig. S1†) owing to the lack of alkyl side chains. But impressively, they all can be well dispersed in *N*-methyl pyrrolidone (NMP) to form stable colloidal solutions (Fig. S2†), which is in line with our previous report on NMP-dispersed colloidal CPs.[36]

The chemical structures of these CPs were confirmed by Fourier transformed infrared (FT-IR) and solid-state ^{13}C NMR spectra (Fig. 1). For FT-IR spectra, all CPs display similar peaks at ~1091 and ~1632 cm^{-1}, which are assigned, respectively, to the skeletal vibrations of aromatic rings and the C–O–C stretching vibrations of EDOT units. BSO_2–EDOT showed a typical peak at 1154 cm^{-1}, corresponding to the stretching mode of the O=S=O groups. DFB–EDOT has a characteristic peak at 1280 cm^{-1} which corresponds to the vibration of the C–F bonds. All CPs evidently retained the characteristic peak of EDOT at ~1632 cm^{-1} (Fig. 1a), suggesting the successful incorporation of EDOT units into CPs. Meanwhile, the peak corresponding to the C–Br characteristic stretching mode of aryl bromides at ~610 cm^{-1} disappeared in all CPs (Fig. S3†), implying that the C–Br bonds have been completely transformed into the C–C bonds by reacting with EDOT.

Fig. 1b shows the solid-state ^{13}C NMR spectra of the CPs. Typically, the signals at 106–118 and 118–154 ppm are attributed to the aromatic 3° and 4° carbons, respectively. DBT–EDOT and BSO_2–EDOT have the same number of carbons and very similar chemical shifts, except that BSO_2–EDOT exhibited a slight shift to high fields caused by the uneven distribution of electrons arising from the electron-withdrawing sulfone group. For DFB–EDOT, the signal at 154 ppm is attributed to the carbons adjacent to F atoms. Note that all as-prepared CPs exhibit an evident peak at ~65 ppm corresponding to the methylene carbon signals of EDOT, which further proves that EDOT has been successfully integrated into all CPs *via* DArP.

The morphology and microstructure of the as-prepared CPs were probed by scanning electron microscopy (SEM) and transmission electron microscopy (TEM). SEM images (Fig. 2) showed that BSO_2–EDOT, DBT–EDOT, and DFB–EDOT exhibited similar layer-stacked morphologies with smooth surfaces, while Py–EDOT exhibited an interlaced rod-like structure.

For comparison, two types of samples, *i.e.*, bulk dispersions in MeOH (Fig. S1†) and colloidal dispersions in NMP (Fig. S2†), were subjected to TEM measurements, respectively (Fig. S4†). In contrast to the bulk particles, the NMP-dispersed colloidal CPs exhibit morphologies of semi-transparent ultra-thin sheets with a size up to hundreds of nanometers. Atomic force microscopy

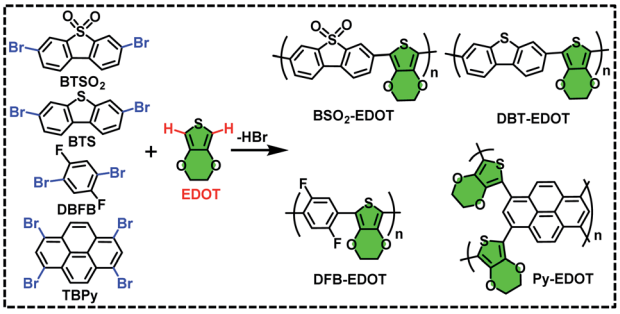

Scheme 1 Synthetic routes for BSO_2–EDOT, DBT–EDOT, Py–EDOT, and DFB–EDOT *via* C–H direct arylation polymerization.

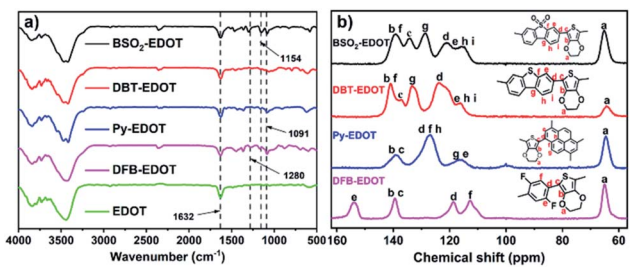

Fig. 1 (a) FT-IR spectra and (b) solid-state ^{13}C NMR spectra of the as-prepared CPs.

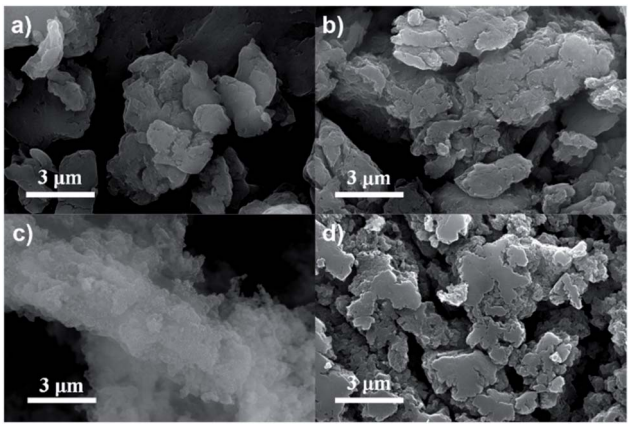

Fig. 2 SEM images of (a) BSO_2–EDOT, (b) DBT–EDOT, (c) Py–EDOT, and (d) DFB–EDOT.

(AFM) further verified the sheet-like morphologies of NMP-dispersed colloidal CPs with a thickness of ~10 nm and width >100 nm (Fig. S5†), implying that NMP exerts an exfoliation effect on CPs.[36] The NMP-dispersed colloidal CPs checked by the dynamic light scattering (DLS) method revealed size distributions of hundreds to thousand nanometers (Fig. S6†), which are in the same order of magnitude with the diameters of nanosheets observed by TEM and AFM. Typically, compared with bulk particles, the colloidal nanoparticles have better dispersibility which will facilitate light harvesting and exciton dissociation on the photocatalyst surface.[37–41] The NMP-exfoliated nanosheets with enlarged specific surface areas and shortened exciton diffusion pathways should be beneficial to expose surface-active sites and improve charge dissociation, thereby enhancing the photocatalytic activity.

Optical and electrochemical properties

The optical and electrochemical properties of the EDOT-based CPs (Fig. 3) were investigated by UV-vis diffuse reflectance spectroscopy (DRS), cyclic voltammetry (CV), photoluminescence (PL), transient photocurrent response (TPR), and calculations based on density functional theory (DFT). All CPs exhibited a broad light response between 300 and 600 nm (Fig. 3a), which is beneficial to visible light harvesting and charge transfer between frontier molecular orbitals (FMOs), and thus promote photocatalysis. Among the CPs, Py–EDOT has the widest light absorption, followed by DFB–EDOT, BSO_2–EDOT, and DBT–EDOT. This absorption trend is directly reflected by the colors of CPs: deeper colors corresponding to better absorbance toward longer wavelengths (insets in Fig. 3a). Correspondingly, the optical bandgaps (E_g) of BSO_2–EDOT, DBT–EDOT, Py–EDOT, and DFB–EDOT derived from the Tauc plots (Fig. S7†) are 2.13, 2.29, 2.03, and 2.07 eV, respectively. Note that the π skeletons of DBT–EDOT and BSO_2–EDOT are much alike except that BSO_2–EDOT has an electron-withdrawing O=S=O group instead of the S atom. This minor modification on DBT–EDOT, however, endows BSO_2–EDOT with a red-shift and broader light absorption (Fig. 3a) owing to the improved D–A (EDOT → BSO_2) intramolecular charge transfer (ICT).

The FMOs of CPs were estimated by CV measurements (Fig. S8†). The highest occupied molecular orbital (HOMO) energy levels were obtained from the oxidation potential in CV curves, and the lowest unoccupied molecular orbital (LUMO) energy levels were calculated based on E_g and HOMOs: $E_{LUMO} = E_{HOMO} + E_g$. Fig. 3b shows the corresponding energy band diagrams of the CPs. The LUMO levels of all CPs intrinsically have sufficient driving forces for proton reduction.

To investigate the photogenerated charge recombination, the steady-state PL spectra of CPs were checked (Fig. 3c). Among the CPs, BSO_2–EDOT has the lowest PL intensity, followed by Py–EDOT, DBT–EDOT and DFB–EDOT, implying that BSO_2–EDOT with a D–A architecture can inhibit radiative recombination more effectively. Furthermore, the photoelectric responses of CPs were evaluated by transient photocurrent response (TPR). The photocurrent–time (I–t) curves under visible light irradiation (Fig. 3d) show that BSO_2–EDOT exhibits the highest photocurrent response: ~1.1 μA cm^{-2} with several on–off cycles, suggesting that the photogenerated charge carriers can be efficiently transported.

DFT calculations were performed to reveal the distributions of FMOs (Table S1†). The HOMOs of all CPs are mainly distributed on the EDOT unit owing to its intrinsic electron-donating character. Among them, BSO_2–EDOT has a more prominent HOMO–LUMO separation compared to other CPs. The LUMO of BSO_2–EDOT is mainly localized on the electron-accepting BSO_2 unit, which leads to less overlap between the HOMO and LUMO, and thus reduces the probability of electron–hole recombination.

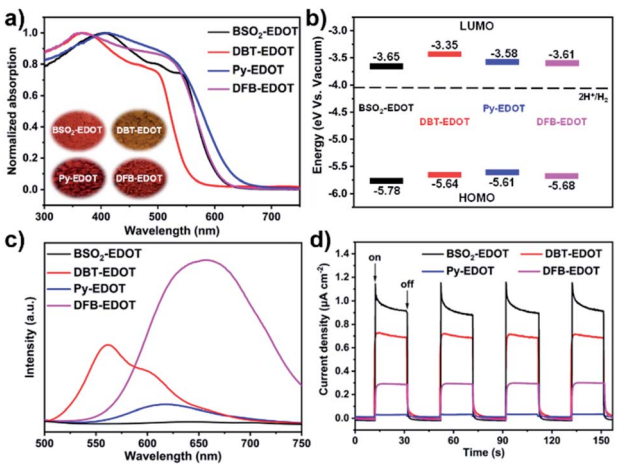

Fig. 3 (a) UV-vis DRS (inset: photographs of CPs). (b) Energy band diagrams. (c) Steady state PL spectra. (d) Transient photocurrents of CPs under visible light irradiation.

Photocatalytic H_2 production and mechanism analysis

The outstanding light absorption, appropriate FMO levels and colloidal character of CPs in NMP encouraged us to investigate their PHP performance, which was carried out under visible light irradiation ($\lambda > 420$ nm) in the absence of the Pt co-catalyst, wherein ascorbic acid (AA) was employed as a sacrificial

electron donor (SED) and water-soluble NMP worked as a co-solvent to improve the dispersibility of CPs.[29,36] Fig. 4 shows the PHP performances of CPs and corresponding apparent quantum yield (AQY) values. As shown in Fig. 4a and Table S2,† all CPs (6 mg) dispersed in H_2O/NMP/AA mixed solution exhibited promising performance, among which, BSO_2–EDOT exhibited the highest HER up to 0.95 mmol h^{-1}, followed by DBT–EDOT (0.39 mmol h^{-1}), DFB–EDOT (0.13 mmol h^{-1}) and Py–EDOT (0.07 mmol h^{-1}), corresponding to the normalized values of 158.4, 65.7, 22.4, and 11.0 mmol h^{-1} g^{-1}, respectively. Fig. 4b shows that the CPs dispersed in AA/H_2O/NMP exhibit 1.5–44 times higher HER than the dispersions in AA/H_2O/MeOH, which are mainly ascribed to the exfoliation effect in NMP (Fig. S2, S4 and S5†),[37] yielding colloidal CPs that possess more exposed active sites and a shorter migration distance of charge carriers compared to their bulk counterparts in MeOH. Meanwhile, NMP can also serve as a medium to create a favorable environment for the PHP reaction. As an aprotic bipolar solvent having a hydrogen bond-accepting group of carbonyls (C═O), NMP exerts a hydrogen bond non-covalent interaction with protons (Fig. S9†), which facilitates the dissociation of the O–H bond, thus decreasing the activation energy of the PHP process.[28,29,42]

Note that BSO_2–EDOT achieves the highest HER among the linear CP photocatalysts, and outperforms most of the reported organic semiconductor photocatalysts (Table S3, ESI†). To unravel the reason behind this, first, a comparison study was made between our D–A copolymer BSO_2–EDOT and the homopolymers, *i.e.*, PEDOT and $PBSO_2$ (with exclusive donor unit EDOT and acceptor unit BSO_2, respectively). BSO_2–EDOT showcased a much higher HER than the reported $PBSO_2$,[43–45] while PEDOT under the same experimental conditions had no PHP activity (Table S4†). The effectiveness of this D–A structure is also reflected by the comparison between BSO_2–EDOT and DBT–EDOT, both of which have closely similar π skeletons (Scheme 1), but BSO_2–EDOT exhibited a HER 2.5 times higher than that of D_1–D_2 type DBT–EDOT (Fig. 4a). These comparisons evidently demonstrate that D–A type BSO_2–EDOT with EDOT as the donor and BSO_2 as the acceptor is highly favorable for PHP, owing to the presence of push–pull D–A interaction,[46–50] improved exciton diffusion, and enhanced electron transfer for proton reduction. Besides, BSO_2–EDOT with the D–A ICT effect led to a much broader absorption toward visible light compared to either D_1–D_2 type DBT–EDOT (Fig. 3a) or A-type $PBSO_2$,[43–45] which also accounts for its excellent HER.

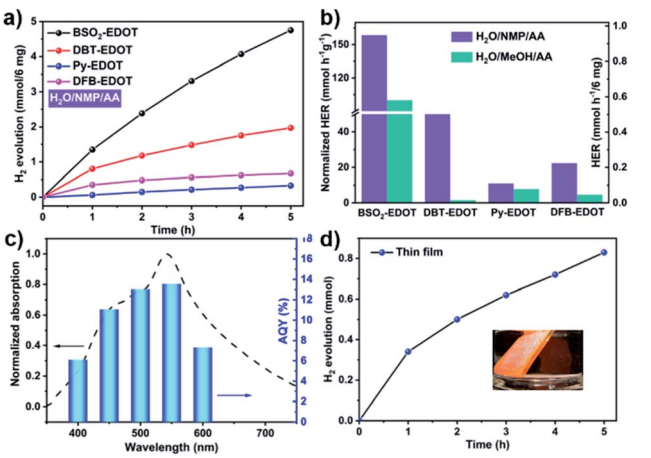

Fig. 4 (a) PHP as a function of time for 6 mg CPs under visible light irradiation. (b) Normalized HERs of CPs dispersed in AA/H_2O/NMP and AA/H_2O/MeOH. (c) AQYs of PHP for BSO_2–EDOT at five different incident light wavelengths. (d) PHP from H_2O for the BSO_2–EDOT film (inset: film photograph) [typical conditions for PHP: 6 mg CPs dispersed in a mixed solution containing 30 ml H_2O, 5 g SED, and 3 ml NMP under visible light irradiation at 25 °C].

Secondly, considering the long-term stability of the NMP-based colloidal solutions of CPs (Fig. S2†), we also investigated their dispersibility in H_2O/NMP (5/1, v/v) mixed solvents (Fig. S10†) which were the same as those used for PHP tests. All the as-prepared CPs can be well dispersed in H_2O/NMP upon ultrasonication. After three days of standing, BSO_2–EDOT can still retain the colloidal state (Fig. S10a†), which may be due to the polar sulfone groups in BSO_2–EDOT. We proposed that sulfone (O═S═O), as a hydrogen bond-acceptor group, can form hydrogen bonds with H_2O, and thus have a solvation stabilization effect on colloidal BSO_2–EDOT (Fig. S10b†), which will promote the PHP process between the catalyst surface and H_2O. Meanwhile, DLS measurement revealed that BSO_2–EDOT has the smallest diameter (Fig. S6†), which may increase its total available surface area for proton reduction. To sum it up, the excellent light harvesting, D–A architecture, and the nano-sized colloidal character in H_2O/NMP mixed solvent rendered BSO_2–EDOT as one of the best photocatalysts toward PHP.

To understand the correlation between PHP and light absorbance, the apparent quantum yields (AQYs) were measured for the BSO_2–EDOT/H_2O/NMP/AA mixture under various mono-chromatic light irradiations (Fig. 4c). The AQYs of BSO_2–EDOT (6 mg) were 6.1%, 11.0%, 13.0%, 13.6%, and 7.3% at 400, 450, 500, 550 and 600 nm, respectively, which matched well with the UV-vis spectrum of the colloidal solution, indicating that the reduction of proton is driven by light irradiation. And a record AQY value of 13.6% at 550 nm was achieved for BSO_2–EDOT. Most of the previously reported highest AQYs were below 500 nm wavelengths (Table S3†). However, the light wavelength window between 500–600 nm constitutes the largest fraction of energy in the solar spectrum. BSO_2–EDOT exhibits the highest AQY in this region and thus yields excellent HERs.[37] Correspondingly, BSO_2–EDOT under visible light irradiation had a comparable HER with the one under full-arc irradiation (0.95 *vs.* 1.06 mmol h^{-1}, Fig. S11†), because the absorbance of BSO_2–EDOT is mainly located in the visible light region (Fig. 3a), and thus UV fraction, *i.e.* $\lambda < 420$ nm, has a limited contribution to its light harvesting ability (Fig. 4c).

The stability of BSO_2–EDOT for PHP was assessed by cycling experiments lasting for 20 h with each cycle of 5 h (Fig. S12†). More impressively, the PHP activity of BSO_2–EDOT after each cycle can be facilely recovered by simple sonication of the colloidal dispersion and replenishment of AA. After the fourth run over a period of 20 h, a HER of 0.66 mmol h^{-1} can be obtained, which was still higher than that of most of the organic photocatalysts (Table S3†). The control experiments on BSO_2–

EDOT/NMP/AA in the absence of H_2O exhibited no hydrogen evolution, implying that the H_2 produced in the above PHP tests did come from H_2O, instead of AA or NMP.

The PHP process of BSO_2–EDOT was visually demonstrated by both balloon-inflating and water-displacing experiments. In the balloon-inflating experiment, 3 mg colloid-like BSO_2–EDOT can even generate $6 \times 5 \times 5$ cm^3 hydrogen gas in 5 h from H_2O under visible light irradiation (ESI Video 1†), and the actual volume of H_2 may be larger than this value because of the tension of the balloon. Concurrent with the balloon-inflating experiment, the water-displacing experiment revealed that 100 ml H_2 can be amazingly produced by 3 mg BSO_2–EDOT within 3 h, and such a surprisingly high HER can be maintained for at least 3 cycles for 9 h (ESI Video 2†). All the above experiments unambiguously demonstrate that BSO_2–EDOT does feature excellent PHP activity. Inspired by the widely used PEDOT-based conductive films,[16–22] here, BSO_2–EDOT was processed into a film by drop casting the NMP-based colloidal dispersion onto a glass substrate, which still retained the intrinsic activity of the photocatalyst (Fig. 4d). Under visible light irradiation in the presence of H_2O and AA, the BSO_2–EDOT-based film is initially covered with small bubbles, which then stably overflow from the surface (ESI Video 3†). A respectable HER of 132.2 mmol h^{-1} m^{-2} was successfully achieved. Considering that the oxygen generation half-reaction is a four-electron pathway that is relatively difficult to achieve by a single semiconductor, BSO_2–EDOT here developed may be used to construct heterojunctions with a second semiconductor[51,52] that have a deep-lying valence band, which will provide opportunity for efficient overall water splitting.

C–H direct arylation *vs.* classical Stille coupling

In parallel with DArP, tin-functionalized EDOT, *i.e.* 2,5-bis(trimethylstannyl)-3,4-ethylenedioxythiophene (bi-Sn-EDOT), together with $BTSO_2$ or DBT was subjected to C–Sn/C–Br Stille coupling polymerization reactions, yielding St–BSO_2–EDOT and St–DBT–EDOT, respectively (Scheme S1† and Fig. 5) for the comparison study. The reaction rates for C–H/C–Br coupling of EDOT were surprisingly fast with obvious colour changes even in ten minutes (Fig. 5a and c) and were comparable to those of the classical Stille couplings (Fig. 5b and d).

More impressively, the PHP activities of both DArP-derived BSO_2–EDOT and DBT–EDOT are superior to those of their Stille-derived counterparts, *i.e.*, 0.95 *vs.* 0.91 mmol h^{-1} for BSO_2–EDOT and St–BSO_2–EDOT, and 0.39 *vs.* 0.26 mmol h^{-1} for DBT–EDOT and St–DBT–EDOT (Fig. S13†), which were contrary to our previous results.[30] These findings demonstrate that EDOT has high reactivity toward DArP, yielding high-performance CPs with sufficient polymerization degrees. Moreover, DArP without the inclusion of Sn precursors also contributes to the superior PHP compared with the Stille-derived counterparts, because tin residues in photocatalysts might have a negative effect on PHP.[53]

EDOT *vs.* thiophene

To gain deeper insights into the effectiveness of EDOT for DArP, $BTSO_2$ with thiophene (Th) or 2,5-bis(trimethylstannyl) thiophene (bi-Sn-Th) was subjected to DArP and Stille polymerization, yielding BSO_2–Th and St–BSO_2–Th, respectively (Scheme S2†). PHP tests showed that DArP-derived BSO_2–Th had a much lower HER than that of the Stille-derived St–BSO_2–Th (0.08 *vs.* 0.38 mmol h^{-1}, Fig. S14†), which was contrary to the above EDOT-based CPs, owing to the relatively low reactivity of thiophene toward DArP, and the undesired reaction on β-C–H bonds of thiophene to form branched side products.

Although the chemical structures of thiophene-based BSO_2–Th and EDOT-based BSO_2–EDOT are closely similar, BSO_2–Th exhibited much lower HERs than that of BSO_2–EDOT (0.39 *vs.* 0.95 mmol h^{-1}, Fig. S14†). UV-vis DRS showed that BSO_2–EDOT has an obvious red-shift and broader visible light absorption compared with BSO_2–Th (Fig. S15†), which means that BSO_2–EDOT can capture more photons in the visible region. The red shift in UV-vis DRS of BSO_2–EDOT is mainly ascribed to its stronger ICT arising from the stronger electron-donating ability of EDOT. The p–π conjugation between the O–C bonds at the 3,4-positions endows EDOT with a ${}^{10}_{7}\prod$ electron-rich system (*i.e.*, 7 atoms share 10 electrons), and thus a stronger electron-donating ability than the thiophene unit (with a ${}^{6}_{5}\prod$ conjugation system).

Moreover, considering that the surface wettability is essential to aqueous photocatalysis, especially for organic photocatalysts,[30,31,41,54–56] here, the water wettability of BSO_2–Th and BSO_2–EDOT was investigated. As shown in Fig. 6, the water contact angle of BSO_2–EDOT (42.3°) was much smaller than that

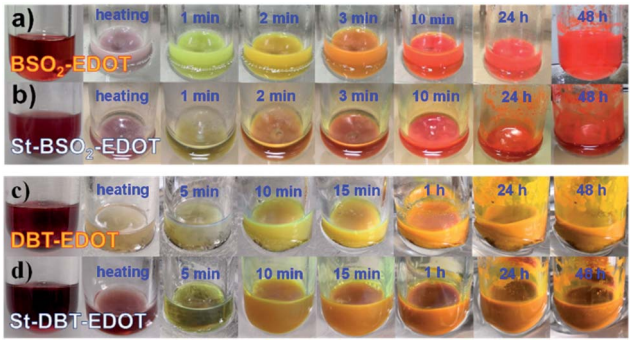

Fig. 5 Color changes of reaction mixtures with time: BSO_2–EDOT synthesized *via* (a) DArP and (b) Stille coupling and DBT–EDOT synthesized *via* (c) DArP and (d) Stille coupling.

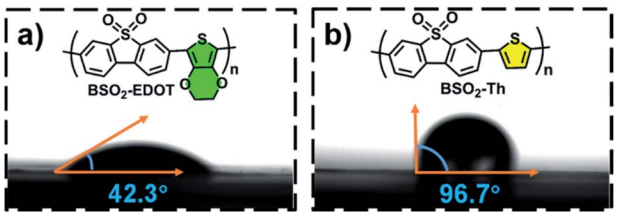

Fig. 6 Water contact angles of (a) BSO_2–EDOT and (b) BSO_2–Th.

of BSO_2–Th (96.7°) owing to the presence of the polar C–O bond[41,54,55] from the ethylene-dioxy substituent, which stressed the pivotal role of EDOT to enhance the hydrophilicity of CPs. As a result, a better interfacial water wettability is achieved for EDOT-based CPs (Fig. 6a), facilitating the accessibility of active sites toward proton reduction.

Effect of residual Pd on PHP performance

Owing to the insolubility of BSO_2–EDOT, the removal of Pd *via* post-treatments by gel permeation chromatography[57,58] or a chelating agent[59] was not possible. To study the effect of residual Pd, five batches of BSO_2–EDOT were synthesized, respectively, by using 0.5, 1.5, 2.5, 3.5 and 5 mol% $Pd_2(dba)_3$ catalyst for DArP. The residual Pd determined by ICP-OES was in the range of 0.16 to 1.24 wt%. The corresponding HERs of these five BSO_2–EDOTs showed no linear relationship with the residual Pd contents (Fig. S16†). The lowest HER of BSO_2–EDOT *via* 0.5 mol% $Pd_2(dba)_3$ was mainly ascribed to the insufficient degree of DArP by too low amount of Pd-catalysts. With the increase of the $Pd_2(dba)_3$ amount, the degree of DArP became normal, while the HERs fluctuated in the range of 0.76 to 1.08 mmol h^{-1} (Fig. S16†) instead of linear enhancement, indicating that there might be a threshold for the content of Pd.[57,58,60] Considering the facts that EDOT-based CPs dispersed in NMP/H_2O have a much higher HER than the ones dispersed in MeOH/H_2O (Fig. 4b), and BSO_2–EDOT outperforms other EDOT-counterparts (Fig. 4a) and BSO_2–Th, we proposed that the following three factors, *i.e.*, the combination of polar sulfone groups[61] with hydrophilic EDOT (Fig. 6), the presence of NMP–H_2O hydrogen bond non-covalent interaction (Fig. S9†),[29,42] and the colloidal character of BSO_2–EDOT in NMP/H_2O,[36] should have more positive effects on the best-performing BSO_2–EDOT than residual Pd.

Conclusions

Four EDOT-based new CPs have been facilely prepared *via* an atom-economic DArP strategy. PHP tests showed that all these EDOT-based CPs mediate considerable HERs under visible light irradiation without additional Pt co-catalysts, among which BSO_2–EDOT with a D–A architecture exhibited the highest HER up to 0.95 mmol h^{-1}, and unprecedented AQY values of 11.1–13.6% within 450–550 nm. The remarkable HERs were both demonstrated instrumentally using standard devices and visually using home-made setups, which showed that 3 mg of colloidal BSO_2–EDOT even produced 100 ml of H_2 (ESI Videos†). Comprehensive comparative studies[62] demonstrated that simple EDOT features many outstanding merits (Fig. S17†), including high stability, excellent reactivity toward DArP with high regioselectivity, water wettability, and enhanced electron-donating ability by O–C p–π conjugation, which make it an attractive electron-donating unit for CP photocatalysts. We envision that more EDOT-based CPs will be synthesized and applicable to all kinds of photocatalytic reactions beyond PHP, such as CO_2 reduction, N_2 fixation, and organic transformations. Meanwhile, the EDOT-based CPs might be combined with other semiconductors to construct heterojunctions for overall water splitting.

Experimental

Materials

TBPy (98%), DBFB (98%), EDOT (98%), thiophene (98%), Cs_2CO_3 (99.9%), P(*o*-MeOPh)$_3$ (98%), $Pd_2(dba)_3$ (98%), PivOH (99%), AA (98%), sodium ascorbate (SA) (98%), DMF (AR), and NMP (AR) were purchased from Energy Chemical Ltd (Shanghai, China). $BTSO_2$ (98%) was purchased from TCI. BTS (98%) was purchased from Alfa Aesar. bi-Sn-EDOT (98%) and bi-Sn-Th (98%) were purchased from SunaTech Inc. (Suzhou, China) and Derthon Co., Ltd (Shenzhen, China), respectively. MeOH (AR) and toluene (AR) were purchased from XiLong Scientific (Shanghai, China).

Typical procedure for the synthesis of CPs *via* DArP[28,35]

A Schlenk tube was charged with the monomers, P(*o*-MeOPh)$_3$, Cs_2CO_3, pivalic acid, and $Pd_2(dba)_3$. The mixed solid in the tube was purged by repetitions of vacuum and argon filling (×3). Then anhydrous toluene was added into the tube *via* a syringe. The reaction mixture was put through freeze–vacuum–thaw cycles three times to remove dissolved gases, and then vigorously stirred at 100 °C for 48 h under an argon atmosphere. After cooling to room temperature, the mixture was poured into CH_2Cl_2. The precipitate was collected by filtration and washed with CH_2Cl_2, MeOH, and distilled water. Further purification of the polymers was carried out by soaking with MeOH and CH_2Cl_2, respectively, and the final powder products were obtained by drying in a vacuum oven at 70 °C for 12 h.

Typical procedure for the synthesis of CPs *via* Stille coupling

A Schlenk tube was charged with the monomers, $Pd_2(dba)_3$ and P(*o*-MeOPh)$_3$. The mixed solid in the tube was purged by repetitions of vacuum and argon filling (×3). Then anhydrous toluene together with a small amount of anhydrous DMF were added into the tube *via* a syringe, respectively. The reaction mixture was put through freeze–vacuum–thaw cycles three times to remove dissolved gases, and then vigorously stirred at 120 °C for 48 h under an argon atmosphere. After cooling to room temperature, the mixture was poured into CH_2Cl_2. The precipitate was collected by filtration and washed with CH_2Cl_2, MeOH, saturated NaF solution, distilled water, and MeOH. Further purification of the polymers was carried out by soaking with CH_2Cl_2, MeOH, saturated NaF solution, distilled water, and MeOH, respectively, and the final powder products were obtained by drying in a vacuum oven at 70 °C for 12 h.

Synthesis of BSO_2–EDOT *via* DArP

$BTSO_2$ (0.535 mmol, 200.0 mg), EDOT (1 equiv., 0.535 mmol, 76.0 mg), Cs_2CO_3 (2 equiv., 1.07 mmol, 348.6 mg), PivOH (30 mol%, 16.4 mg), $Pd_2(dba)_3$ (1.5 mol%, 7.3 mg), P(*o*-MeOPh)$_3$ (3 mol%, 5.7 mg), and 7 ml anhydrous toluene were used to synthesize BSO_2–EDOT *via* DArP. The product was obtained as an orange-red powder (176.5 mg, 93.2%). Elem. Anal for

$(C_{18}H_{10}O_4S_2)_n$ (%): C 61.00; H 2.84; S 18.09. Found: C 58.35; H 3.22; S 19.28.

Synthesis of DBT–EDOT *via* DArP

BTS (0.584 mmol, 200.0 mg), EDOT (1 equiv., 0.584 mmol, 83.2 mg), Cs_2CO_3 (2 equiv., 1.168 mmol, 381.0 mg), PivOH (30 mol%, 17.9 mg), $Pd_2(dba)_3$ (1.5 mol%, 10.7 mg), P(*o*-MeOPh)$_3$ (3 mol%, 8.2 mg), and 7 ml anhydrous toluene were used to synthesize DBT–EDOT *via* DArP. The product was obtained as a yellow powder (172.5 mg, 91.4%). Elem. Anal for $(C_{18}H_{10}O_2S_2)_n$ (%): C 67.06; H 3.13; S 19.89. Found: C 63.16; H 3.07; S 20.05.

Synthesis of Py–EDOT *via* DArP

TBPy (0.386 mmol, 200.0 mg), EDOT (2 equiv., 0.772 mmol, 109.8 mg), Cs_2CO_3 (2 equiv., 1.544 mmol, 503.1 mg), PivOH (30 mol%, 23.6 mg), $Pd_2(dba)_3$ (1.5 mol%, 14.1 mg), P(*o*-MeOPh)$_3$ (3 mol%, 10.9 mg), and 7 ml anhydrous toluene were used to synthesize Py–EDOT *via* DArP. The product was obtained as a dark-red powder (174.3 mg, 94.3%). Elem. Anal for $(C_{28}H_{16}O_4S_2)_n$ (%): C 69.98; H 3.36; S 13.34. Found: C 68.43; H 3.06; S 12.56.

Synthesis of DFB–EDOT *via* DArP

DBFB (0.736 mmol, 200.0 mg), EDOT (1 equiv., 0.736 mmol, 104.6 mg), Cs_2CO_3 (2 equiv., 1.472 mmol, 479.4 mg), PivOH (30 mol%, 22.5 mg), $Pd_2(dba)_3$ (1.5 mol%, 13.5 mg), P(*o*-MeOPh)$_3$ (3 mol%, 10.4 mg), and 7 ml anhydrous toluene were used to synthesize DFB–EDOT *via* DArP. The product was obtained as a red powder (168.1 mg, 90.6%). Elem. Anal for $(C_{12}H_6F_2O_2S)_n$ (%): C 57.14; H 2.40; S 12.71. Found: C 54.08; H 2.29; S 12.06.

Synthesis of St–BSO_2–EDOT *via* Stille coupling

$BTSO_2$ (0.535 mmol, 200.0 mg), bi-Sn-EDOT (1 equiv., 0.535 mmol, 250.3 mg), $Pd_2(dba)_3$ (2 mol%, 9.8 mg), P(*o*-MeOPh)$_3$ (4 mol%, 7.5 mg), 7 ml anhydrous toluene, and 0.1 ml anhydrous DMF were used to synthesize St–BSO_2–EDOT *via* Stille coupling. The product was obtained as an orange-red powder (148.9 mg, 78.5%). Elem. Anal for $(C_{18}H_{10}O_4S_2)_n$ (%): C 61.00; H 2.84; S 18.09. Found: C 58.26; H 2.64; S 17.52.

Synthesis of St–DBT–EDOT *via* Stille coupling

BTS (0.585 mmol, 200.0 mg), bi-Sn-EDOT (1 equiv., 0.585 mmol, 273.7 mg), $Pd_2(dba)_3$ (2 mol%, 10.7 mg), P(*o*-MeOPh)$_3$ (4 mol%, 8.2 mg), 7 ml anhydrous toluene, and 0.1 ml anhydrous DMF were used to synthesize St–DBT–EDOT *via* Stille coupling. The product was obtained as a yellow powder (144.0 mg, 76.3%). Elem. Anal for $(C_{18}H_{10}O_2S_2)_n$ (%): C 67.06; H 3.13; S 19.89. Found: C 64.63; H 3.01; S 18.45.

Synthesis of BSO_2–Th *via* DArP

$BTSO_2$ (0.535 mmol, 200.0 mg), thiophene (1 equiv., 0.535 mmol, 45.0 mg), $Pd_2(dba)_3$ (2 mol%, 9.8 mg), P(*o*-MeOPh)$_3$ (4 mol%, 7.5 mg), 7 ml anhydrous toluene, and anhydrous 0.1 ml DMF were used to synthesize BSO_2–Th *via* DArP. The product was obtained as a yellow green powder (90.6 mg, 57.2%). Elem. Anal for $(C_{16}H_8O_2S_2)_n$ (%): C 64.85; H 2.72; S 21.64. Found: C 60.82; H 2.34; S 19.76.

Synthesis of St–BSO_2–Th *via* Stille coupling

$BTSO_2$ (0.535 mmol, 200.0 mg), bi-Sn-Th (1 equiv., 0.535 mmol, 219.2 mg), $Pd_2(dba)_3$ (2 mol%, 9.8 mg), P(*o*-MeOPh)$_3$ (4 mol%, 7.5 mg), 7 ml anhydrous toluene, and 0.1 ml anhydrous DMF were used to synthesize St–BSO_2–EDOT *via* Stille coupling. The product was obtained as an orange-red powder (144.6 mg, 91.2%). Elem. Anal for $(C_{16}H_8O_2S_2)_n$ (%): C 64.85; H 2.72; S 21.64. Found: C 63.01; H 2.58; S 20.52.

Hydrogen evolution tests

The typical PHP test was performed in a photocatalytic online analysis system (LabSolar-III AG, Beijing Perfect Light) linked with a gas chromatograph (GC9790, FuLi). First, the as-prepared photocatalysts (6 mg) were ultrasonically dispersed in 6 ml NMP for 30 min, and then the suspension was transferred into a mixed aqueous solution containing 30 ml H_2O, 2.5 g AA, and 2.5 g SA. SA was used to adjust the pH to 4.0, a similar value to the pKa of AA.[30] The mixture was degassed to remove the dissolved air before irradiation using an oil pump. Then, the reactor was irradiated by using a 300 W Xe lamp (Beijing Perfect Light, PLS-SXE300) equipped with a 420 nm cut-off filter; the reaction temperature was fixed at 25 °C using a flow of cooling water. The amount of hydrogen produced was analyzed by using a gas chromatograph equipped with a thermal conductive detector (TCD) using argon as the carrier gas.

Balloon-inflating and water-displacing experiments were carried out with a 25 ml Schlenk tube. The Schlenk tube contained 3 mg photocatalysts and 3 ml NMP, which were ultrasonically dispersed for 30 min, and then the mixed aqueous solution containing 15 ml H_2O, 1.3 g AA and 1.3 g SA was added. The Schlenk tube was put through freeze–vacuum–thaw cycles three times to remove dissolved gases and lastly filled with 1 atm pressure of argon, and then stirred for the PHP test under visible light irradiation. The detailed set-up can be found in ESI Videos 1 and 2.†

Hydrogen evolution test of the BSO_2–EDOT film

BSO_2–EDOT (3 mg) powder was added into NMP (1 ml) and ultrasonically dispersed for 30 min. The obtained dispersion was drop cast onto glass and dried at 75 °C for 3 h. Then, the yielded BSO_2–EDOT-based film was immersed in a mixed aqueous solution containing 30 ml H_2O, 2.5 g AA, and 2.5 g SA for the PHP test under visible light irradiation (ESI Video 3†). After that, the film can be dried and recycled.

Data availability

All data needed to evaluate the conclusions in the paper are present in the paper and/or ESI.†

Author contributions

Z.-R. T. performed and analyzed the experiments and contributed to the writing of the original draft. Y.-Q. X. J.-Z. C., Z.-Q. S. and Y. J. Z. performed part of the experiments. Z.-R. T., G. Z., G. L., L. C. and S.-Y. L. analyzed the data and prepared the manuscript. S.-Y. L. supervised and conceptualized the project, funding acquisition, provided guidance during all stages, and contributed to the writing of the manuscript.

Conflicts of interest

There are no conflicts to declare.

Acknowledgements

The National Natural Science Foundation of China (Nos 21374075 and 22169009), Jiangxi Provincial Natural Science Foundation (No. 20212ACB204007) and the Jiangxi Provincial Key Laboratory of Functional Molecular Materials Chemistry (20212BCD42018) are acknowledged for financial support. The authors thank Prof. Ai-Guo Zhong for DFT calculations.

Notes and references

1 Y. Tachibana, L. Vayssieres and J. R. Durrant, *Nat. Photon.*, 2012, **6**, 511–518.
2 A. Fujishima and K. Honda, *Nature*, 1972, **238**, 37–38.
3 X. Chen, S. Shen, L. Guo and S. S. Mao, *Chem. Rev.*, 2010, **110**, 6503–6570.
4 T. Banerjee, F. Podjaski, J. Kröger, B. P. Biswal and B. V. Lotsch, *Nat. Rev. Mater.*, 2020, **6**, 168–190.
5 J. Bi, W. Fang, L. Li, J. Wang, S. Liang, Y. He, M. Liu and L. Wu, *Macromol. Rapid Commun.*, 2015, **36**, 1799–1805.
6 X. Wang, K. Maeda, A. Thomas, K. Takanabe, G. Xin, J. M. Carlsson, K. Domen and M. Antonietti, *Nat. Mater.*, 2009, **8**, 76–80.
7 G. Zhang, Z. A. Lan and X. Wang, *Angew. Chem., Int. Ed.*, 2016, **55**, 15712–15727.
8 R. S. Sprick, J. X. Jiang, B. Bonillo, S. Ren, T. Ratvijitvech, P. Guiglion, M. A. Zwijnenburg, D. J. Adams and A. I. Cooper, *J. Am. Chem. Soc.*, 2015, **137**, 3265–3270.
9 Y. O. Wang, A. Vogel, M. Sachs, R. S. Sprick, L. Wilbraham, S. J. A. Moniz, R. Godin, M. A. Zwijnenburg, J. R. Durrant, A. I. Cooper and J. W. Tang, *Nat. Energy*, 2019, **4**, 746–760.
10 L. Stegbauer, K. Schwinghammer and B. V. Lotsch, *Chem. Sci.*, 2014, **5**, 2789–2793.
11 J. Kosco, F. Moruzzi, B. Willner and I. McCulloch, *Adv. Energy Mater.*, 2020, **10**, 2001935.
12 Y. Li, Y. Wang, C. L. Dong, Y. C. Huang, J. Chen, Z. Zhang, F. Meng, Q. Zhang, Y. Huang, D. Zhao, L. Gu and S. Shen, *Chem. Sci.*, 2021, **12**, 3633–3643.
13 X. Li, P. M. Maffettone, Y. Che, T. Liu, L. Chen and A. I. Cooper, *Chem. Sci.*, 2021, **12**, 10742–10754.
14 A. J. Heeger, *Chem. Soc. Rev.*, 2010, **39**, 2354–2371.
15 Z. Zheng, H. Yao, L. Ye, Y. Xu, S. Zhang and J. Hou, *Mater. Today*, 2020, **35**, 115–130.
16 L. Groenendaal, F. Jonas, D. Freitag, H. Pielartzik and J. R. Reynolds, *Adv. Mater.*, 2000, **12**, 481–494.
17 Y. H. Kim, C. Sachse, M. L. Machala, C. May, L. Muller-Meskamp and K. Leo, *Adv. Funct. Mater.*, 2011, **21**, 1076–1081.
18 H. Shi, C. C. Liu, Q. L. Jiang and J. K. Xu, *Adv. Electron. Mater.*, 2015, **1**, 1500017.
19 L. V. Kayser and D. J. Lipomi, *Adv. Mater.*, 2019, **31**, 1806133.
20 Y. Y. Jiang, T. F. Liu and Y. H. Zhou, *Adv. Funct. Mater.*, 2020, **30**, 2006213.
21 Y. Liang, A. Offenhausser, S. Ingebrandt and D. Mayer, *Adv. Healthcare Mater.*, 2021, **10**, 2100061.
22 Y.-Q. Zheng, Y. Liu, D. Zhong, S. Nikzad, S. Liu, Z. Yu, D. Liu, H.-C. Wu, C. Zhu, J. Li, H. Tran, J. B.-H. Tok and Z. Bao, *Science*, 2021, **373**, 88–94.
23 P. Anastas and N. Eghbali, *Chem. Soc. Rev.*, 2010, **39**, 301–312.
24 S.-Y. Liu, M.-M. Shi, J.-C. Huang, Z.-N. Jin, X.-L. Hu, J.-Y. Pan, H.-Y. Li, A. K. Y. Jen and H.-Z. Chen, *J. Mater. Chem. A*, 2013, **1**, 2795–2805.
25 J. R. Pouliot, F. Grenier, J. T. Blaskovits, S. Beaupre and M. Leclerc, *Chem. Rev.*, 2016, **116**, 14225–14274.
26 N. S. Gobalasingham and B. C. Thompson, *Prog. Polym. Sci.*, 2018, **83**, 135–201.
27 T. Bura, S. Beaupre, M. A. Legare, J. Quinn, E. Rochette, J. T. Blaskovits, F. G. Fontaine, A. Pron, Y. Li and M. Leclerc, *Chem. Sci.*, 2017, **8**, 3913–3925.
28 W.-Y. Huang, Z.-Q. Shen, J.-Z. Cheng, L.-L. Liu, K. Yang, X.-R. Chen, H.-R. Wen and S.-Y. Liu, *J. Mater. Chem. A*, 2019, **7**, 24222–24230.
29 J.-Z. Cheng, L.-L. Liu, G. Liao, Z.-Q. Shen, Z.-R. Tan, Y.-Q. Xing, X.-X. Li, K. Yang, L. Chen and S.-Y. Liu, *J. Mater. Chem. A*, 2020, **8**, 5890–5899.
30 R. S. Sprick, B. Bonillo, R. Clowes, P. Guiglion, N. J. Brownbill, B. J. Slater, F. Blanc, M. A. Zwijnenburg, D. J. Adams and A. I. Cooper, *Angew. Chem., Int. Ed.*, 2016, **55**, 1792–1796.
31 X. Wang, L. Chen, S. Y. Chong, M. A. Little, Y. Wu, W. H. Zhu, R. Clowes, Y. Yan, M. A. Zwijnenburg, R. S. Sprick and A. I. Cooper, *Nat. Chem.*, 2018, **10**, 1180–1189.
32 C. Shu, C. Han, X. Yang, C. Zhang, Y. Chen, S. Ren, F. Wang, F. Huang and J. X. Jiang, *Adv. Mater.*, 2021, **33**, 2008498.
33 C. M. Aitchison, M. Sachs, M. A. Little, L. Wilbraham, N. J. Brownbill, C. M. Kane, F. Blanc, M. A. Zwijnenburg, J. R. Durrant, R. S. Sprick and A. I. Cooper, *Chem. Sci.*, 2020, **11**, 8744–8756.
34 C. Han, P. Dong, H. Tang, P. Zheng, C. Zhang, F. Wang, F. Huang and J. X. Jiang, *Chem. Sci.*, 2021, **12**, 1796–1802.
35 S.-Y. Liu, D.-G. Wang, A.-G. Zhong and H.-R. Wen, *Org. Chem. Front.*, 2018, **5**, 653–661.
36 J.-Z. Cheng, Z.-R. Tan, Y.-Q. Xing, Z.-Q. Shen, Y.-J. Zhang, L.-L. Liu, K. Yang, L. Chen and S.-Y. Liu, *J. Mater. Chem. A*, 2021, **9**, 5787–5795.
37 J. Kosco, M. Bidwell, H. Cha, T. Martin, C. T. Howells, M. Sachs, D. H. Anjum, S. Gonzalez Lopez, L. Zou, A. Wadsworth, W. Zhang, L. Zhang, J. Tellam, R. Sougrat, F. Laquai, D. M. DeLongchamp, J. R. Durrant and I. McCulloch, *Nat. Mater.*, 2020, **19**, 559–565.

38 C. H. Dai, Y. T. Pan and B. Liu, *Adv. Energy Mater.*, 2020, **10**, 2002474.
39 C. M. Aitchison and R. S. Sprick, *Nanoscale*, 2021, **13**, 634–646.
40 R. L. Li, N. C. Flanders, A. M. Evans, W. Ji, I. Castano, L. X. Chen, N. C. Gianneschi and W. R. Dichtel, *Chem. Sci.*, 2019, **10**, 3796–3801.
41 J. Kosco, S. Gonzalez-Carrero, C. T. Howells, W. Zhang, M. Moser, R. Sheelamanthula, L. Zhao, B. Willner, T. C. Hidalgo, H. Faber, B. Purushothaman, M. Sachs, H. Cha, R. Sougrat, T. D. Anthopoulos, S. Inal, J. R. Durrant and I. McCulloch, *Adv. Mater.*, 2021, 2105007.
42 W.-C. Lin, J. Jayakumar, C.-L. Chang, L.-Y. Ting, M. H. Elsayed, M. Abdellah, K. Zheng, A. M. Elewa, Y.-T. Lin, J.-J. Liu, W.-S. Wang, C.-Y. Lu and H.-H. Chou, *Appl. Catal., B*, 2021, **298**, 120577.
43 M. Sachs, R. S. Sprick, D. Pearce, S. A. J. Hillman, A. Monti, A. A. Y. Guilbert, N. J. Brownbill, S. Dimitrov, X. Shi, F. Blanc, M. A. Zwijnenburg, J. Nelson, J. R. Durrant and A. I. Cooper, *Nat. Commun.*, 2018, **9**, 4968.
44 C. M. Aitchison, R. S. Sprick and A. I. Cooper, *J. Mater. Chem. A*, 2019, **7**, 2490–2496.
45 G. Shu, Y. Li, Z. Wang, J.-X. Jiang and F. Wang, *Appl. Catal., B*, 2020, **261**, 118230.
46 Z. A. Lan, W. Ren, X. Chen, Y. F. Zhang and X. C. Wang, *Appl. Catal., B*, 2019, **245**, 596–603.
47 W. Chen, L. Wang, D. Mo, F. He, Z. Wen, X. Wu, H. Xu and L. Chen, *Angew. Chem., Int. Ed.*, 2020, **59**, 16902–16909.
48 Z. Q. Sheng, Y. Q. Xing, Y. Chen, G. Zhang, S. Y. Liu and L. Chen, *Beilstein J. Nanotechnol.*, 2021, **12**, 607–623.
49 J. Zhao, J. Ren, G. Zhang, Z. Zhao, S. Liu, W. Zhang and L. Chen, *Chem.–Eur. J.*, 2021, **27**, 10781–10797.
50 Q. Xie, Y. Yang, W. Zhang, Z. Gao, X. Li, J. Tang, C. Pan and G. Yu, *Chem. Sci.*, 2021, **12**, 5631–5637.
51 A. Wadsworth, Z. Hamid, J. Kosco, N. Gasparini and I. McCulloch, *Adv. Mater.*, 2020, **32**, 2001763.
52 G. Liao, C. Li, S.-Y. Liu, B. Fang and H. Yang, *Trends Chem.*, 2022, **4**(2), 111–127.
53 R. S. Sprick, C. M. Aitchison, E. Berardo, L. Turcani, L. Wilbraham, B. M. Alston, K. E. Jelfs, M. A. Zwijnenburg and A. I. Cooper, *J. Mater. Chem. A*, 2018, **6**, 11994–12003.
54 Z. Hu, Z. Wang, X. Zhang, H. Tang, X. Liu, F. Huang and Y. Cao, *iScience*, 2019, **13**, 33–42.
55 Y. Bai, Z. Hu, J. X. Jiang and F. Huang, *Chem.–Asian J.*, 2020, **15**, 1780–1790.
56 S. Zhang, G. Cheng, L. Guo, N. Wang, B. Tan and S. Jin, *Angew. Chem., Int. Ed.*, 2020, **59**, 6007–6014.
57 J. Kosco, M. Sachs, R. Godin, M. Kirkus, L. Francas, M. Bidwell, M. Qureshi, D. Anjum, J. R. Durrant and I. McCulloch, *Adv. Energy Mater.*, 2018, **8**, 1802181.
58 J. Kosco and I. McCulloch, *ACS Energy Lett.*, 2018, **3**, 2846–2850.
59 K. T. Nielsen, K. Bechgaard and F. C. Krebs, *Macromolecules*, 2005, **38**, 658–659.
60 L. Li, Z. Cai, Q. Wu, W. Y. Lo, N. Zhang, L. X. Chen and L. Yu, *J. Am. Chem. Soc.*, 2016, **138**, 7681–7686.
61 M. Sachs, H. Cha, J. Kosco, C. M. Aitchison, L. Francas, S. Corby, C. L. Chiang, A. A. Wilson, R. Godin, A. Fahey-Williams, A. I. Cooper, R. S. Sprick, I. McCulloch and J. R. Durrant, *J. Am. Chem. Soc.*, 2020, **142**, 14574–14587.
62 Comparisons including BSO_2–EDOT *vs.* PEDOT & $PBSO_2$, BSO_2–EDOT *vs.* DBT–EDOT, DArP *vs.* Stille coupling, and BSO_2–EDOT *vs.* BSO_2–Th, see Fig. 5 and 6, Tables S3 and S4 and Fig. S13 and S15.†